Article

Ultrafast Impact Superspreading on Superamphiphilic Silicon Surfaces for Effective Thermal Management

Zhongpeng Zhu, Yupeng Chen, Xianfeng Luo, Weining Miao, Zhichao Dong, Jiajia Zhou, Ye Tian,* and Lei Jiang
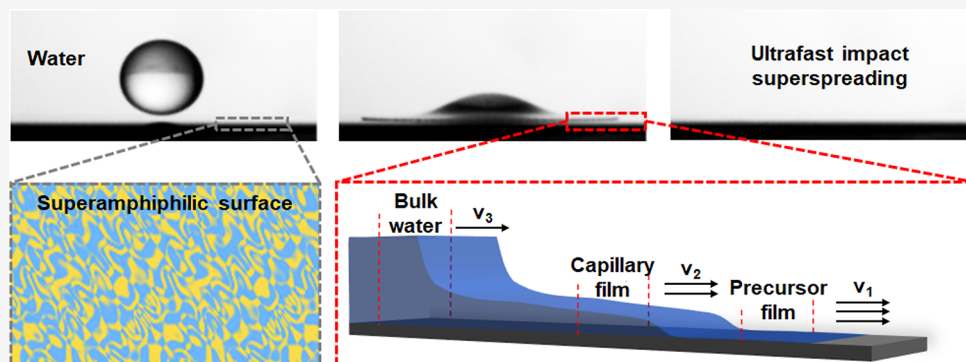
Read Online

ACCESS | 📊 Metrics & More | 📰 Article Recommendations | 🆘 Supporting Information

ABSTRACT: Controllable impact spreading behavior is critical for effective thermal management of spray cooling. However, splash and retraction are common problems on hydrophobic (HPB) and hydrophilic (HPL) surfaces. Herein, by regulation of surface wettability, we report a controllable ultrafast impact superspreading behavior (superspreading time of ∼3.0 ms) without splash and retraction on superamphiphilic (SAPL) silicon surfaces. Analysis of dynamic wetting processes combined with observation of lateral force microscopy images on SAPL surfaces reveals the existence of a precursor film at the spreading edge induced by heterogeneous surface wettability at nanoscale. Further study indicates that the inhibition of splash results from the high liquid flux in precursor film, which suppresses the interposition of air at the spreading edge. The reduction of Laplace forces owing to the presence of precursor film inhibits retraction at the spreading frontier. Taking advantage of this impact superspreading behavior on SAPL surfaces, effective heat dissipation is demonstrated, offering uniform and high heat flux for the spray cooling process.

■ INTRODUCTION

With the decrease of size and increase of power for modern electronics, thermal management has become a critical prerequisite to maintain device efficiency and reliability.[1−3] By atomizing the cooling agent into microscale droplets and impacting hot substrates, spray cooling exhibits high heat dissipation efficiency and temperature uniformity.[4] However, during the liquid impact process, the splash of liquid droplets result in inhomogeneous heat dissipation and the retraction of spread liquid film reduces the liquid−solid contact area, which hinder the improvement of heat transfer efficiency during the spray cooling process.[5−8] Hence, it is significant to study the liquid impact behavior to achieve controllable liquid deposition, which is crucial for thermal management of spray cooling, but also significant for various industrial applications, such as reducing the waste of pesticide in agriculture, improving the precision of patterns during inkjet printing, fabricating uniform functional films by drop-casting, *and so forth.*[9−12]

To achieve controllable liquid deposition without splash and retraction, three main factors during the impact process are commonly considered, namely, environmental condition, liquid property, and state of substrate.[13] Typical studies of environmental conditions revealed that the corona splash can be suppressed by reducing air pressure.[14] Regulation of liquid properties such as impact velocity, liquid viscosity, surface energy, and so forth shows various methods to suppress splash and retraction.[15−17] Besides, using soft or inclined substrates can inhibit the splash process.[18−20] However, in applications that involve the liquid impact spreading process like printing and spray cooling, regulation of surface wettability to achieve controllable superspreading is preferred, which offers several advantages, such as improved printing precision, reduced liquid loss, increased heat dissipation efficiency, and so forth.[21,22]
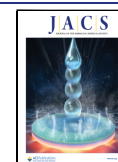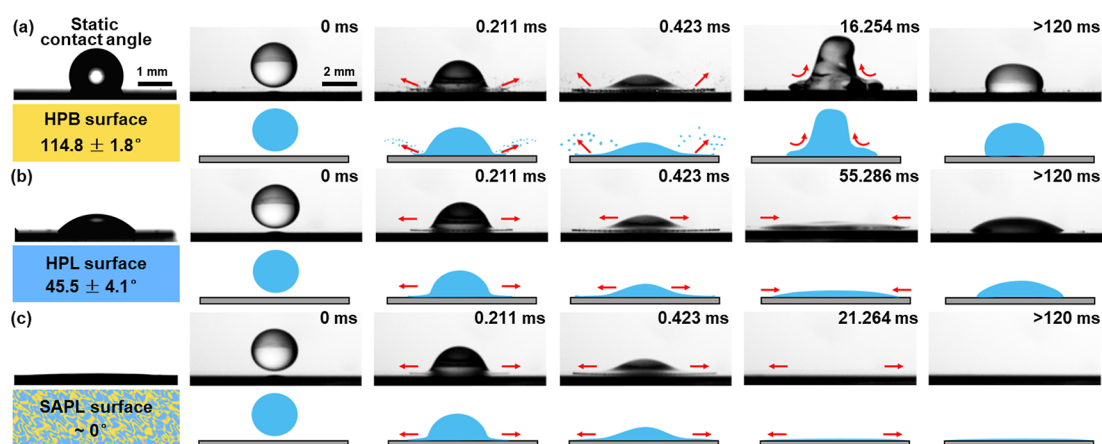
Figure 1. Comparison of impact behavior for water droplets on substrates with various wettabilities. (a) Water droplets' impact on hydrophobic (HPB) surfaces with static water contact angles of $114.8 \pm 1.8°$ showed prompt splash and partially rebound behaviors. (b) Water droplets' impact on hydrophilic (HPL) surfaces with water contact angles of $45.5 \pm 4.1°$ showed curved spreading with retraction behaviors. (c) Water droplets' impact on superamphiphilic (SAPL) silicon surfaces with water contact angles around $0°$ showed impact superspreading behaviors without splash and retraction.
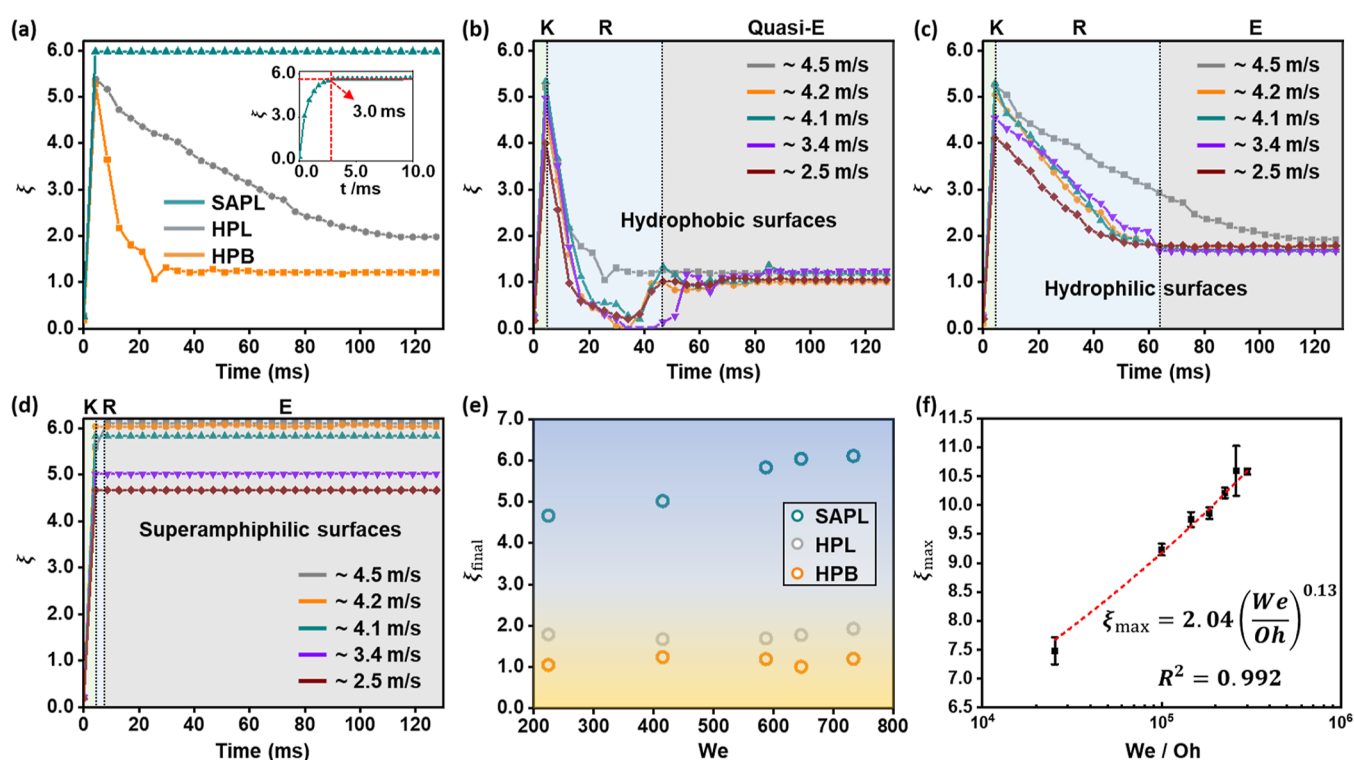

Figure 2. Analysis of the impact process on substrates with various wettabilities at different impact speeds. (a) Non-dimensional spreading radius (ξ) over time curves are recorded for the impact behaviors of water droplets with constant velocity on various substrates, and inset reveals the ultrafast superspreading behavior on SAPL silicon surfaces with the superspreading time of around 3.0 ms. (b) Impact rebound behaviors of water droplets on HPB surfaces. (c) Impact with retraction behaviors of water droplets on HPL surfaces. (d) Impact superspreading behaviors of water droplets on SAPL silicon surfaces. (e) Final non-dimensional spreading radius (ξ_{final}) on various substrates with different wettabilities at various Weber (We) numbers was analyzed indicating the ξ_{final} on SAPL silicon surfaces increases with the increase of We and can reach 6. (f) Fitted curve of the maximum non-dimensional spreading radius (ξ_{max}) varies with We and Ohnesorge number (Oh), indicating the liquid spreads without undergoing shear.

Previous studies are mostly focused on hydrophilic (HPL), hydrophobic (HPB), and superhydrophobic surfaces, on which impact superspreading is hard to achieve. Hence, the study of surface wettability to achieve impact superspreading with simultaneous suppression of splash and retraction is still a challenge.

Herein, by regulation of surface wettability, a controllable ultrafast impact superspreading behavior without splash and retraction is revealed on superamphiphilic (SAPL) silicon surfaces. The ultrafast impact superspreading process exhibits a superspreading time of around 3.0 ms, which is defined as the time from the droplet contacts the solid substrate to its final spreading state when the three-phase contact line pins.

Compared with impact behaviors on HPL and HPB surfaces, the final superspreading area increases with the increase of the impact speed on SAPL silicon surfaces. Calculations of the spreading factors combined with the lateral force microscopy images further revealed the existence of a precursor film on SAPL silicon surfaces, resulting from the two-dimensional capillary forces induced by alternating HPL and HPB nano-domains. The liquid flux of precursor film at the spreading edge is much higher than the bulk liquid droplet, hence the splash is effectively suppressed on SAPL silicon surfaces. Force analysis at the spreading frontier indicated that the horizontal Laplace pressure acting as the retraction force decreases with the improvement of surface wettability, and the retraction behavior is also inhibited after the formation of precursor film. Taking advantage of the impact superspreading behavior on SAPL silicon surfaces, effective heat dissipation is demonstrated, which shows uniform and high heat flux during the spray cooling process.

■ RESULTS AND DISCUSSION

Impact behaviors of water droplets are recorded by a high-speed camera at atmospheric pressure with a relatively high impact velocity of ~4.5 m/s on HPB, HPL, and SAPL surfaces. HPB and HPL surfaces are prepared on silicon substrates by a physical vapor deposition method. SAPL silicon surfaces are prepared by a modified RCA cleaning method, and various liquids can all spread on SAPL silicon surfaces with static contact angles near 0° (Figure S1). Water droplets on HPB surfaces with static water contact angles of $114.8 \pm 1.8°$ splashed and spread with wrinkles at the spreading frontier at the initial stage and then partially rebounded from the surface and finally deposited on the substrate to reach the equilibrium state after 120 ms (Figure 1a). Water droplets' impact on HPL surfaces with static water contact angles of $45.5 \pm 4.1°$ spread with wrinkles at the spreading frontier at the initial stage and then retracted to a static state after 120 ms (Figure 1b). However, water droplets' impact on SAPL silicon surfaces exhibited different behaviors with continuous spreading and no wrinkles at the spreading frontier (Figure 1c). Besides, water droplets can spread completely without retraction on the SAPL silicon surfaces with static water contact angles near 0°. Furthermore, liquids with various surface energy (dimethyl sulfoxide, hexadecane, ethanol, hexane) and impact speeds are also studied with similar impact behaviors to water (Figure ST1). Hence, we focused on water droplets for detailed discussion in this study. The intriguing impact superspreading behavior without splash and retraction of water droplets indicates that the interaction of liquid and substrate is stronger than the insertion of air, which inhibited the separation of spreading liquid lamina from the substrate. To further reveal the differences in impact behaviors of water droplets on HPB, HPL, and SAPL silicon surfaces, various impact processes are recorded with different impact velocities.

To reveal different impact behaviors at surfaces with various wettability, the non-dimensional spreading radius ($\xi = R_t/R_0$, where R_t is the spreading radius and R_0 is the radius of an initial spherical water droplet) ξ versus time curves are recorded at different impact velocities (Figures S2–S4). First, a relatively high impact velocity of ~4.5 m/s was chosen to reveal the distinct impact behaviors at substrates with various surface wettability over 120 ms (Figure 2a). Interestingly, it is found that water droplets showed ultrafast impact super-spreading behavior with a superspreading time of ~3.0 ms on

SAPL silicon surfaces (inset of Figure 2a) with effective suppression of splash and retraction. Furthermore, the impact processes are divided into three typical phases to analyze the detailed impact behaviors, namely, kinetic phase (K-phase), relaxation phase (R-phase), and equilibrium phase (E-phase).[23] The K-phase is defined as the period that begins with the liquid droplet's contact with the solid substrate to its maximum spreading area, during which the impact process is dominated by high kinetic energy of droplet and splash generally occurs. R-phase is defined as the period after the K-phase and before the three-phase contact line pins, during which the receding contact angle plays a critical role and the retraction process occurs. E-phase is defined as the state when the three-phase contact line pins, which is determined by the interfacial force balance of air/solid, air/liquid, and liquid/solid. Water droplets' impact on HPB surfaces showed curved spreading edges at the three-phase contact line during the K-phase, followed by complete rebound behaviors within 50 ms at a relatively low impact velocity (Figure 2b). However, with the increase of impact speed, prompt splash appeared during the K-phase. In this case, the kinetic energy of the water droplet is dissipated, which results in a partial rebound behavior (impact velocity of ~4.5 m/s). After the three-phase contact line pins, the water droplet reached the Quasi-E phase with the pinned water droplet vibrating up and down. The impact behaviors are slightly different on HPL surfaces with an initial splash, impact spread, and retraction processes, as shown in Figure 2c. Water droplets showed splash in K-phase on HPL surfaces at the very initial stage (observed at 0.064 ms), which is inconspicuous compared with the prompt splash on HPB surfaces (Figure S5). The R-phase with retraction behavior on the HPL surface (>60 ms) takes longer than the retraction process on the HPB surface (<50 ms). Besides, when the impact speed of the water droplet is increased to ~4.5 m/s, the time of R-phase with retraction behaviors takes two-fold longer than the process at relatively low velocity.

Distinct from the splash with bounce and spread with retraction behaviors observed on HPB and HPL surfaces, the ultrafast impact superspreading behavior was observed on SAPL surfaces. As shown in Figure 2d, water droplets impacting on SAPL silicon surfaces showed ultrafast impact superspreading behaviors during the K-phase within the initial 3.0 ms and reached their maximum spreading states. After a negligible R-phase, they reached the E-phase almost identical to the maximum spreading areas. It is intriguing to find the spreading edge of the water droplet at the three-phase contact line spreads without wrinkles compared with the spreading behaviors on HPB and HPL surfaces at the instantaneous impact state of 0.423 ms (refers to Figure 1). Besides, it is found that the final spreading areas increase with the increase of the impact speed on SAPL surfaces, which are relatively constant on HPB and HPL surfaces.

Since the final spreading areas are relevant with the impact speed of water droplets on SAPL surfaces, the impact superspreading behavior with a controllable spreading area is further studied. Variation of the final non-dimensional spreading radius (ξ_{final}) versus Weber (We) number, which is only controlled by impact speed, was observed for surfaces with different wettabilities, as shown in Figure 2e. We is defined as $We = \rho v^2 D_0/\gamma$, where ρ is water density, v is impact velocity, D_0 is the droplet diameter, and γ is liquid surface tension. The ξ_{final} showed similar values of around 1 for HPB surfaces and 2 for HPL surfaces, indicating that ξ_{final} is similar
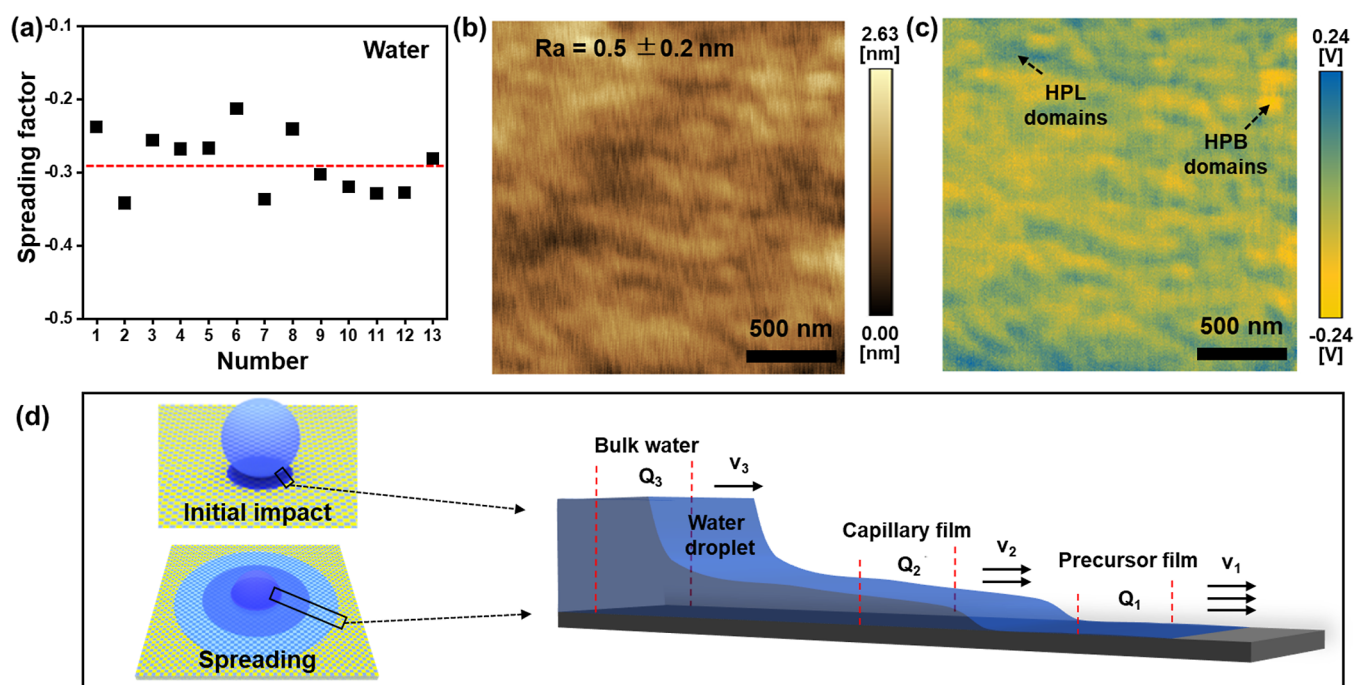
Figure 3. Precursor film-assisted impact superspreading process. (a) Calculation of the spreading factor based on contact angle versus time curve indicates that the spreading process follows Tanner's Law. (b) Height image of the SAPL silicon surface 2.5×2.5 μm^2 showing that the surface is atomic flat with Ra of 0.5 ± 0.2 nm. (c) Lateral force images over 2.5×2.5 μm^2 showing alternating HPL and HPB nano-domains. (d) Schematic diagram of initial and spreading process with the assistance of the precursor film resulting from two-dimensional capillary forces induced by alternating HPL and HPB nano-domains on SAPL silicon surfaces (not in scale). Water flux analysis of impact superspreading process on SAPL silicon surface indicates that the liquid flux per unit length (Q_1) in precursor film is much higher than the liquid flux per unit length in capillary film (Q_2) and bulk water (Q_3).

at substrates with similar wettability and irrelevant to the increase of the We number. However, it is notable that the ξ_{final} increased with We number on SAPL silicon surfaces and the maximum value can reach 6, which is 3-fold larger than the maximum value on HPL surfaces and 6-fold larger than the value of HPB ones. Previous studies reported several different models to analyze the relationship between the maximum non-dimensional spreading radius (ξ_{max}), which is identical to the ξ_{final} on SAPL surfaces in this study. The We/Oh numbers are studied concerning inertia force, liquid viscosity, and surface tension.[24] Oh is Ohnesorge number, which is $Oh = \eta/(\rho D_0 \gamma)^{1/2}$ with η of liquid viscosity. Based on the ξ_{max} over We/Oh numbers for water droplets on SAPL silicon surfaces at various conditions, a fitted curve is revealed, as shown in Figure 2f. The ξ_{max} can be summarized with a nonlinear formula with R^2 of 0.992

$$\xi_{max} = 2.04 \left(\frac{We}{Oh}\right)^{0.13} \tag{1}$$

We number changes with the impact speed of liquid droplet, and Oh number is only affected by the intrinsic property of liquid. It is found that the fitted curve of ξ_{max} versus We/Oh numbers follows the free-spreading process of the "squeeze flow model".[24] The "squeeze flow model" is proposed to explain the liquid jetting process without undergoing shear for large maximum spreading with high impact velocities and low liquid viscosities. In our study, since the water spreading process on the SAPL surface follows the "squeeze flow model", it is inferred that the impact superspreading process also undergoes a no-shear spreading process, which can be explained owing to the existence of an ultra-fast prespread

precursor film ahead of the observed capillary film. Hence, the ξ_{final}, which is identical to ξ_{max}, increases with the increase of liquid impact speeds. Besides, based on this formula, the final maximum superspreading area can also be predicted and controlled by the regulation of We numbers, which is significant for precise ink-jet printing.

Spreading factors calculated based on the contact angle versus time curve are extensively used to analyze the spreading states for the liquid spreading process, which is critically important in various fields.[25−28] In 1979, Tanner reported that when the spreading process of an axisymmetric droplet is driven by wettability and a precursor film involved, the spreading factor is around −0.3.[29] The spreading factor can be calculated based on contact angle versus time curve or spreading radius versus time curve, as shown in Figure S6. In our study, several individual tests are performed and the calculated spreading factors are shown in Figure 3a with an average value of $−0.29 \pm 0.04$ for water droplets impacting on SAPL silicon surfaces, which indicates the spreading process follows Tanner's Law. Hence, it can be concluded that the spreading process of the water droplet on the SAPL silicon surface is driven by surface wettability and there is a thin precursor film (defined as the nano-scale invisible thin film ahead of the visible capillary film).[30] However, the formation mechanism of the precursor film is still unclear. To further reveal the formation mechanism of precursor film on the SAPL silicon surface, atomic force microscopy (AFM) of lateral force mode was applied to study the distribution of surface functional groups and nano-scale surface wettability.[31,32] Previous reports show that there are typically two kinds of functional groups on silicon surfaces with a native oxide layer, namely, hydroxyl group and oxygen bridges.[33] To reveal the
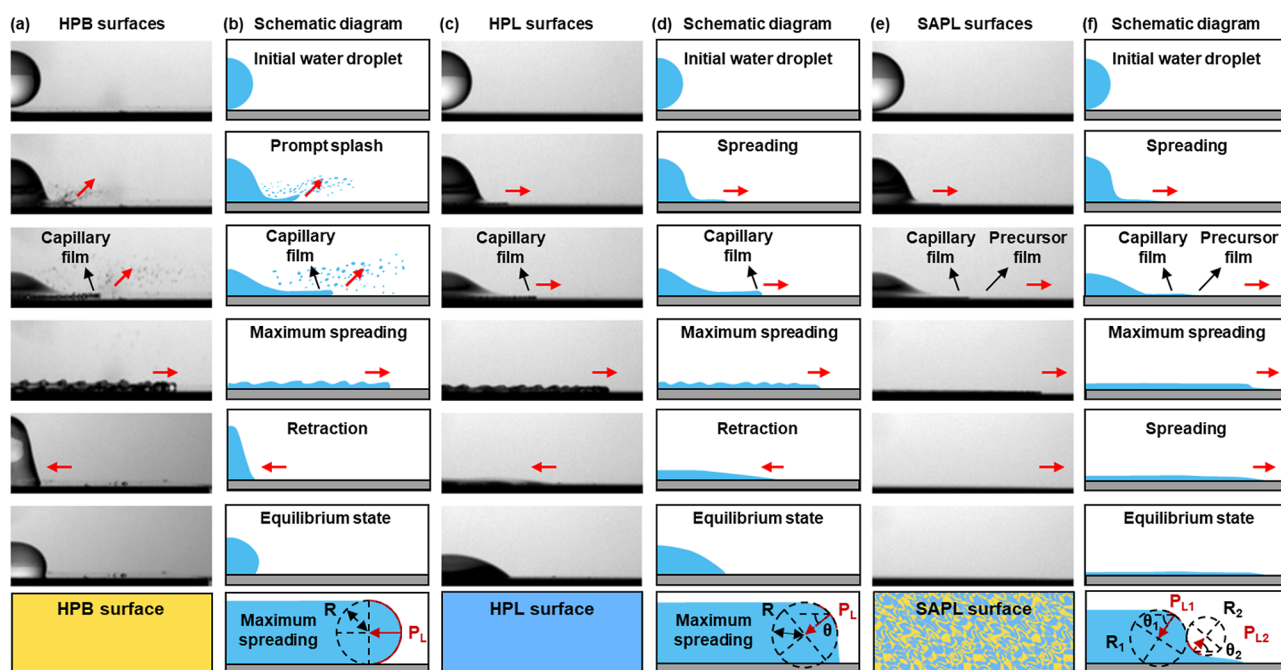
Figure 4. Force analysis at the spreading frontier. (a,b) Optical images and schematic diagrams of water droplets' impact on HPB surfaces with splash and partial rebound behaviors. The schematic diagram at the bottom of (b) shows that capillary film at the maximum spreading state on HPB surfaces results in a strong retraction force owing to the horizontal Laplace pressure (P_L). (c,d) Optical images and schematic diagrams of water droplets' impact on HPL surfaces with spreading and retraction behaviors. The schematic diagram at the bottom of (d) shows that the improved surface wettability results in a curvature of the capillary film on HPL surface and the horizontal P_L is reduced. (e,f) Optical images and schematic diagrams of water droplets' impact on SAPL silicon surfaces with impact superspreading behaviors. The schematic diagram at the bottom of (f) shows that additional P_L forms owing to the existence of precursor film ahead of the capillary film, and the retraction force is greatly reduced.

distribution of these functional groups, an atomic flat SAPL silicon surface is prepared. The AFM height image showed that the silicon surface is atomic flat with surface roughness (Ra) of 0.5 ± 0.2 nm (Figure 3b). Further, a lateral force image revealed an alternating distribution of friction patterns on SAPL silicon surfaces, as shown in Figure 3c. The blue areas with high friction forces represent the HPL nano-domains, and the yellow areas with relatively low friction forces represent the relatively HPB nano-domains.[34] Based on the abovementioned observation, it is inferred that the thin precursor film is induced by the two-dimensional capillary forces resulting from the alternating HPL and HPB nano-domains on SAPL silicon surfaces.

Previous research reported that the splash process is mainly governed by the liquid surface tension and the gas environment.[35] However, in this study, with identical liquid property and environmental circumstances, water droplets showed distinct impact behaviors on HPB, HPL, and SAPL silicon surfaces, which means that the precursor film plays a critical role in the liquid impact process. Besides, molecular dynamic simulations revealed that the precursor film forms almost at the initial state when the droplet contacts the solid surface.[36] Hence, a precursor film-assisted impact superspreading process is proposed to explain the ultrafast impact superspreading behavior on SAPL silicon surfaces, as the schematic diagram shown in Figure 3d. The schematic diagram illustrates the spreading frontier of the very initial impact state and the "straw hat" spreading state. During both of these spreading processes, there are two parts spreading ahead of the bulk water droplet, namely, the visible capillary film with thickness at micro-scale and the precursor film with thickness at nano-scale or sub-nanoscale.[36,37] During the ultrafast impact spreading process of

water droplets, a thin precursor film would spread with a relatively higher speed ahead of the capillary film owing to the two-dimensional capillary forces. Herein, Q is defined as the cross-section liquid flux per unit length during unit time. Hence, the liquid flux in precursor film (Q_1) is higher than the liquid flux in capillary film (Q_2). In turn, Q_2 is higher than the liquid flux in the bulk water droplet (Q_3). Because of the existence of a thin precursor film spread ahead of the visible capillary film, air cannot insert between the liquid film and solid substrate, which effectively suppresses splashing on SAPL silicon surfaces. In contrast, owing to the poor surface wettability water droplets can more easily splash on HPL and HPB surfaces (also refer to Figure S6). Besides, the spreading edge of the water droplet at the three-phase contact line spreads without wrinkles on SAPL silicon surfaces compared with HPL and HPB surfaces, which may be the critical factor for retraction behaviors of capillary films.

Force analysis of the Laplace pressure (P_L) acting on spreading frontier is critically important for both static and dynamic wetting processes. It is reported that the liquid filament ahead of a spreading liquid stripe affects force interaction at the three-phase contact line and determines drop emission.[38] By enlarged observation of the spreading frontier during the impact process of water droplets, it is inferred that the horizontal P_L in the capillary film changes with the improvement of surface wettability near the three-phase contact line. As shown in Figure 4a, after the water droplet impact on HPB surfaces, the capillary film showed prompt splash and then retracted. In this study, the prompt splash was observed on HPB surfaces immediately after water impact and the thin capillary film breaks into tiny droplets injected upward. The remained capillary film spreads with wrinkles at
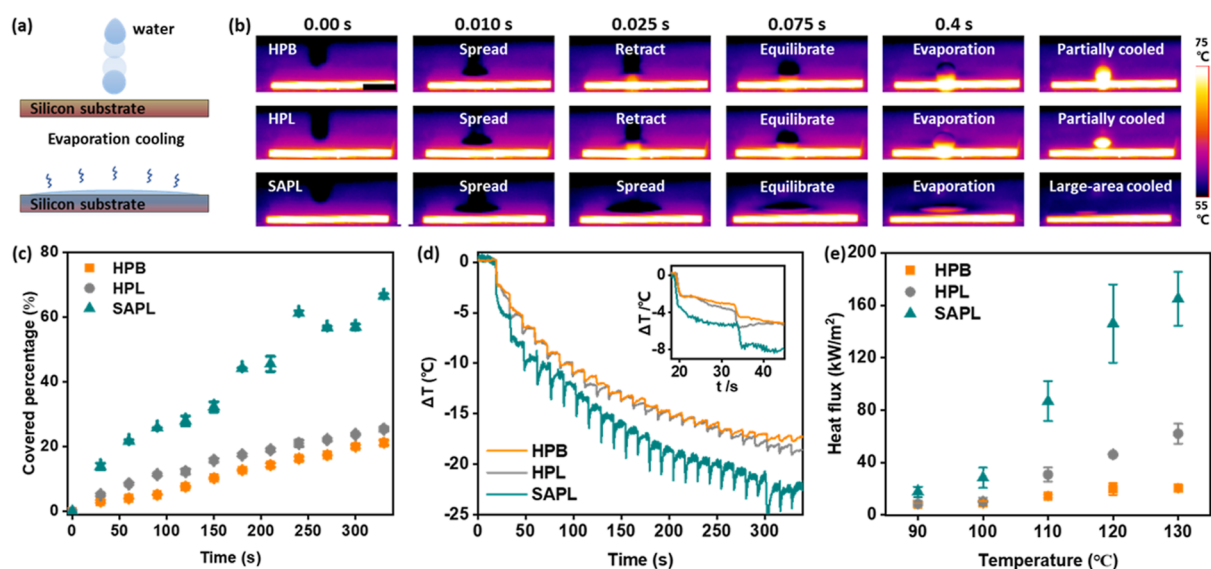
Figure 5. Impact superspreading-enhanced effective heat dissipation. (a) Schematic diagram illustrates the impact superspreading-enhanced heat dissipation process for a single water droplet. (b) Inferred camera images show detailed evolution of heat dissipation during the impact process on substrates with different wettabilities. Scale bar is 5 mm. (c) Covered percentage over time for continuous deposition of single water droplets on the substrate with different wettabilities. (d) Average temperature change of substrates with different wettabilities for continuous water droplet deposition, and insets show the rapid temperature change in the initial stage. (e) Heat flux over a heated area of 2×2 cm^2 is estimated by $q = mL/\tau A$, which indicates that the SAPL surfaces outperform HPB and HPL surfaces.

the spreading edge until it reaches the maximum spreading state. Then owing to the hydrophobic property of the substrates, the capillary film holds a large contact angle, which results in a strong P_L at horizontal as the schematic diagram shown at the bottom in Figure 4b. In this case, the retraction force, which results from the additional P_L, can be described as $P_L = 2\gamma/R$, with R as the radius of curvature for the spreading tip. This retraction force drives the liquid film to retract until it reaches the equilibrium hydrophobic state.

For water droplet impact on HPL surfaces, the liquid droplet spreads initially with a slightly curved spreading edge until it reaches the maximum spreading state and then slowly retracts to its equilibrium HPL state, as shown in Figure 4c. It is noticed that compared with the morphology of capillary film on HPB surfaces, when the water droplet reaches its maximum spreading state, the thickness of capillary film on HPL surfaces is relatively thin and the dynamic contact angle at the edge is relatively small. As shown at the bottom of the schematic diagram of Figure 4d, the horizontal P_L is reduced owing to the improved surface wettability of solid substrates, which can be expressed as $P_L = (2\gamma \cos\theta)/R$, with θ being the angle between the Laplace force and the horizontal. In this case, the retraction force is relatively small compared with the retraction force on HPB surfaces. In turn, the retraction process takes a longer time (>60 ms) on HPL surfaces than the retraction process on HPB ones (<50 ms).

Distinctly from the impact behaviors on HPB and HPL surfaces, impact behaviors on SAPL surfaces exhibit an impact superspreading behavior, as shown in Figure 4e. The water droplet continues spreading without wrinkles at the spreading edge, which is due to the existence of a thin precursor film, as the schematic diagram shows in Figure 4f. Due to the formation of additional spreading force (P_{L2}) resulting from the precursor film ahead of the capillary film, the retraction force (P_{L1}) is greatly reduced, which results in the continuous superspreading behavior without wrinkles at the spreading edge on SAPL silicon surfaces. Detailed analysis of the P_L

revealed that the total force that acts at the three-phase contact line can be expressed as follows: $P_L = P_{L1} - P_{L2} = (2\gamma \cos\theta_1)/R_1 - (2\gamma \cos\theta_2)/R_2$, with R_1 being the radius of curvature for capillary film, R_2 being the radius of curvature for precursor film, θ_1 being the angle between the Laplace force and the horizontal for capillary film, and θ_2 being the angle between the Laplace force and the horizontal for precursor film. The retraction Laplace force acting on the SAPL surface is reduced by the additional Laplace force induced by the formation of precursor film. Hence, a thin water film can form at the equilibrium state of a water droplet on the SAPL silicon surface. Based on the force analysis at the spreading edge, the retraction behaviors on HPL/HPB surfaces and the superspreading behavior on SAPL silicon surfaces can be explained, and we proposed the precursor film-assisted impact superspreading process to explain the ultrafast impact superspreading behavior on SAPL silicon surfaces.

The heat dissipation efficiency is critically important for spray cooling, which is determined by the evaporation rate and affected by the impact behaviors of cooling agent. Herein, we chose water as the cooling agent owing to its versatility with large latent heat and compared the heat dissipation process on HPB, HPL, and SAPL surfaces. As the schematic diagram shows in Figure 5a, a single water droplet is vertically deposited on the heated silicon substrate with an impact speed of 1−2 m/s, which is close to the situation for practical applications. The substrate can be rapidly cooled as water evaporates along the deposited areas. Detailed evolution of heat dissipation during the impact process is recorded by the inferred camera, as shown in Figure 5b. When the cooling agent (water droplet) impacts HPB and HPL substrates, it will spread initially. Then the spread capillary film will retract, and the three-phase contact line pins, which results in very limited liquid/solid contact areas for heat transfer. In this case, the solid surface can only be partially cooled around the liquid deposited area, while other areas still remain at high temperature. In contrast, the water droplet spreads on SAPL substrates with large liquid/

solid contact areas offering large-area heat transfer, which can effectively cool the whole hot substrate.

Based on the improvement of surface wettability, uniformity of heat transfer can be inferred owing to the increase of covered percentage, which is obtained based on the spreading area of water droplets over the whole substrate area. As shown in Figure 5c, with continuous deposition of single water droplets on substrates around 90 °C of different surface wettabilities, the percentage of covered SAPL surfaces increases to over 60% due to the enhanced spreading process. In contrast, the covered percentage is around 20% for HPL and HPB surfaces, indicating that the solid substrates are partially cooled, which may increase the risk for the formation of outliers or hotspots. The average temperature change of substrates is recorded, as shown in Figure 5d. The surface average temperature is recorded, indicating a rapid decrease around 8 °C, as water droplets are deposited on SAPL surfaces owing to the impact superspreading behavior (inset of Figure 5d). In contrast, the average temperature change of HPB and HPL surfaces decreased around 5 °C. For a relatively long time interval, the average temperature of SAPL surfaces can be around 4 °C lower than HPB and HPL surfaces with continuous deposition of water droplets, which demonstrates that the impact superspreading process can effectively enhance the spry cooling process. Further study evaluated the heat flux during the evaporation-based heat dissipation process over a heated area of 2×2 cm^2. The heat flux discussed in this study is calculated with $q = mL/\tau A$ (m is the drop mass, L is the latent heat of water at 0.1 MPa and 100 °C, τ is the evaporation time, and A is the substrate area), which is a comprehensive result concerning heat transfer from solid substrates, liquids, and the surrounding gas. As shown in Figure 5e, over a temperature range of 90−130 °C, SAPL surfaces show better heat flux than HPB and HPL surfaces. The heat flux for SAPL surfaces is over 3 times higher than that for HPB and HPL surfaces, indicating the effective heat dissipation process, which can be further used in spray cooling.

CONCLUSIONS

In this study, the influence of nano-scale surface wettability on liquid impact behavior is studied on HPB, HPL, and SAPL silicon surfaces. Different from the impact rebound and spread with retraction behaviors on HPB and HPL surfaces, the controllable ultrafast impact superspreading behavior (super-spreading time of around 3.0 ms) occurs on SAPL silicon surfaces without splash and retraction. Analysis of the spreading process at different impact speeds showed that surface wettability influences the whole impact process including kinetic, relaxation, and equilibrium phases. Besides, compared with the impact behaviors on HPB and HPL surfaces, the final spreading area increases with the increase of impact speed on SAPL silicon surfaces. Based on the calculations of spreading factors and observations of lateral force images on SAPL silicon surfaces, a precursor film spreading ahead of the observed capillary film is revealed, which is due to the two-dimensional capillary forces induced by alternating HPL and HPB nano-domains. Moreover, a precursor film-assisted impact superspreading process is proposed. The effective suppression of splash is analyzed concerning liquid flux per unit length of capillary film and precursor film. Besides, the inhibition of retraction is discussed concerning forces at the spreading frontier. Furthermore, the effective heat dissipation process is demonstrated on SAPL

surfaces, which is due to the impact superspreading behaviors and which offers uniform and high heat flux for the spray cooling process. This study demonstrates that the nano-scale surface wettability on SAPL silicon surfaces can simultaneously suppress splash and retraction of water droplets, resulting in an ultrafast impact superspreading behavior, which can effectively improve the evaporation-based heat dissipation process. However, further studies can be extended to applications, where the liquid impact superspreading process is involved and fine control of the spreading area is needed including nano-materials/functional molecule self-assembling and thin-film fabrication for thin-film electronic devices.

MATERIALS AND METHODS

Chemicals and Reagents. N-type silicon wafer polished on one side of <100> ± 0.5° crystal orientation with 0.001−0.005 Ω·cm, 500 ± 10 μm thickness, and 100 ± 0.2 mm diameter was purchased from China Electronics Technology Group Corporation. Deionized water was prepared by a Milli-Q system (Millipore, USA) with a resistivity of 18.2 MΩ·cm at room temperature. Acetone, ethanol, ammonium hydroxide (NH$_4$OH), hydrochloric acid (HCl), hydrogen peroxide (H$_2$O$_2$), and nitric acid (HNO$_3$) were of analytical grade and purchased from Beijing Chemical Reagent Co., Ltd. (1H,1H,2H,2H-heptadecafluorodecyl) trimethoxysilane and (3-Aminopropyl) trime-thoxysilane were purchased from Aladdin. All chemicals are used as received without further treatment.

Preparation of Superamphiphilic Surfaces. Silicon wafer was cut into pieces of 2.0×2.0 cm^2, sonicated, and cleaned sequentially using acetone, ethanol, and deionized water for 10 min. Then these silicon substrates were treated with a modified RCA cleaning method: First, these substrates were immersed in a freshly prepared alkaline hydrogen peroxide solution (step 1: NH$_4$OH/H$_2$O$_2$/H$_2$O (v/v/v) = 1:1:5) for 10 min at 70−80 °C. Then they were rinsed with deionized water and immersed in a freshly mixed hydrochloric hydrogen peroxide solution (step 2: HCl/H$_2$O$_2$/H$_2$O (v/v/v) = 1:1:5) for 10 min at 70−80 °C. Finally, after being rinsed with deionized water, these silicon substrates were treated in HNO$_3$ (65%) for 10 min at room temperature and then kept in deionized water.

Fabrication of Hydrophobic and Hydrophilic Silicon Surfaces. A physical vapor deposition method was applied to fabricate hydrophobic and hydrophilic silicon surfaces. The 2.0×2.0 cm^2 silicon substrates were plasma-treated at 200 W for 300 s. Then the salinization process was carried out in a closed chamber at a concentration of silanes of around 5.0×10^{-3} M under reduced pressure of around 0.2 atm at 120 °C for 4 h to construct a hydrophobic silicon surface with (1H,1H,2H,2H-heptadecafluorodec-yl) trimethoxysilane and a hydrophilic silicon surface with (3-Aminopropyl) trimethoxysilane.[39]

Heat Dissipation Characterizations. The surface temperature is monitored by an A615 inferred camera (FLIR, America). Substrates are heated on the C-MAG HS7 hot stage (IKA, Germany). A single water droplet is applied by the syringe pump at a speed of 2−3 mL/h above the substrate of around 5 cm. The spray cooling process is carried out on the hot stage with a constant wind flow of 1.8 m/s by an electric fan, and water droplets are applied by a sprayer at a distance above the substrate of around 5 cm.

Material Characterizations. The static contact angle measurements were carried out by the OCA20 apparatus (Data-Physics, Germany) with 2 μL of water droplets at room temperature. The lateral force microscopy images were obtained using the SPM-8000 atomic force microscope (Shimadzu, Japan). The AFM tip is N-type signal crystal silicon with a rectangular cantilever, and the force constant is 0.01−0.5 N/m. The normal force applied in the experiment is ∼0.2 nN, and the scan rate is 1−2 Hz. The water droplet impact behaviors were recorded by a Dimax HS4 high-speed camera (PCO, Germany) at a frame rate of around 47,000 fps, and the impact speed was calculated from recorded movies. The exposure time is around 5 μs, and the focal length is around 0.5 m. Liquid

impact speed was controlled by releasing liquid droplets at different heights. Water droplets of diameter between 2.0 and 3.0 mm were released with a stainless-steel needle above the silicon substrate laid horizontally at atmospheric conditions.

ASSOCIATED CONTENT

Supporting Information

The Supporting Information is available free of charge at https://pubs.acs.org/doi/10.1021/jacs.3c01394.

Detailed observation of impact behaviors on hydrophobic, hydrophilic, and superamphiphilic surfaces with various condition, comparison of calculation methods of spreading factors (PDF)

Water droplet impacts on hydrophobic surfaces (AVI)

Water droplet impacts on hydrophilic surfaces (AVI)

Water droplet impacts on superamphiphilic surfaces (AVI)

AUTHOR INFORMATION

Corresponding Author

Ye Tian − *Key Laboratory of Bio-inspired Materials and Interfacial Science, Technical Institute of Physics and Chemistry, Chinese Academy of Sciences, Beijing 100190, China; University of Chinese Academy of Sciences, Beijing 100049, China;* orcid.org/0000-0002-1913-6333; Email: tianyely@iccas.ac.cn

Authors

Zhongpeng Zhu − *University of Science and Technology of China, Hefei 230026, China; Suzhou Institute for Advanced Research, University of Science and Technology of China, Jiangsu 215123, China*

Yupeng Chen − *CAS Key Laboratory for Biomedical Effects of Nanomaterials and Nanosafety, CAS Center for Excellence in Nanosci-ence, National Center for Nanoscience and Technology, Beijing 100190, China*

Xianfeng Luo − *Key Laboratory of Bio-inspired Materials and Interfacial Science, Technical Institute of Physics and Chemistry, Chinese Academy of Sciences, Beijing 100190, China; University of Chinese Academy of Sciences, Beijing 100049, China*

Weining Miao − *Key Laboratory of Bio-inspired Materials and Interfacial Science, Technical Institute of Physics and Chemistry, Chinese Academy of Sciences, Beijing 100190, China; University of Chinese Academy of Sciences, Beijing 100049, China;* orcid.org/0000-0003-2403-6000

Zhichao Dong − *Key Laboratory of Bio-inspired Materials and Interfacial Science, Technical Institute of Physics and Chemistry, Chinese Academy of Sciences, Beijing 100190, China; University of Chinese Academy of Sciences, Beijing 100049, China*

Jiajia Zhou − *South China Advanced Institute for Soft Matter Science and Technology, School of Emergent Soft Matter, South China University of Technology, Guangzhou 510640, China;* orcid.org/0000-0002-2258-6757

Lei Jiang − *University of Science and Technology of China, Hefei 230026, China; Suzhou Institute for Advanced Research, University of Science and Technology of China, Jiangsu 215123, China; Key Laboratory of Bio-inspired Materials and Interfacial Science, Technical Institute of Physics and Chemistry, Chinese Academy of Sciences, Beijing 100190, China; University of Chinese Academy of Sciences,*

Beijing 100049, China; orcid.org/0000-0003-4579-728X

Complete contact information is available at:
https://pubs.acs.org/10.1021/jacs.3c01394

Notes

The authors declare no competing financial interest.

ACKNOWLEDGMENTS

REFERENCES

(1) Zhang, Q.; Lv, Y.; Wang, Y.; Yu, S.; Li, C.; Ma, R.; Chen, Y. Temperature-dependent dual-mode thermal management device with net zero energy for year-round energy saving. *Nat. Commun.* **2022**, *13*, 4874.

(2) Song, H.; Liu, J.; Liu, B.; Wu, J.; Cheng, H.-M.; Kang, F. Two-dimensional materials for thermal management applications. *Joule* **2018**, *2*, 442−463.

(3) Moore, A. L.; Shi, L. Emerging challenges and materials for thermal management of electronics. *Mater. Today* **2014**, *17*, 163−174.

(4) Jiang, M.; Wang, Y.; Liu, F.; Du, H.; Li, Y.; Zhang, H.; To, S.; Wang, S.; Pan, C.; Yu, J.; Quéré, D.; Wang, Z. Inhibiting the Leidenfrost effect above 1,000 °C for sustained thermal cooling. *Nature* **2022**, *601*, 568−572.

(5) Bourrianne, P.; Lv, C.; Quéré, D. The cold Leidenfrost regime. *Sci. Adv.* **2019**, *5*, No. eaaw0304.

(6) Shiri, S.; Bird, J. C. Heat exchange between a bouncing drop and a superhydrophobic substrate. *Proc. Natl. Acad. Sci. U.S.A.* **2017**, *114*, 6930−6935.

(7) Hu, Y.; Lei, Y.; Liu, X.; Yang, R. Heat transfer enhancement of spray cooling by copper micromesh surface. *Mater. Today Phys.* **2022**, *28*, 100857.

(8) Zhu, Z.; Chen, Y.; Xu, Z.; Yu, Z.; Luo, X.; Zhou, J.; Tian, Y.; Jiang, L. Super-spreading on superamphiphilic micro-organized nanochannel anodic aluminum oxide surfaces for heat dissipation. *iScience* **2021**, *24*, 102334.

(9) Zuo, C.; Ding, L. Drop-Casting to Make Efficient Perovskite Solar Cells under High Humidity. *Angew. Chem., Int. Ed.* **2021**, *60*, 11242−11246.

(10) Song, M.; Ju, J.; Luo, S.; Han, Y.; Dong, Z.; Wang, Y.; Gu, Z.; Zhang, L.; Hao, R.; Jiang, L. Controlling liquid splash on superhydrophobic surfaces by a vesicle surfactant. *Sci. Adv.* **2017**, *3*, No. e1602188.

(11) Yarin, A. L. Drop impact dynamics: Splashing, spreading, receding, bouncing. *Annu. Rev. Fluid. Mech.* **2006**, *38*, 159−192.

(12) Derby, B. Inkjet printing of functional and structural materials: Fluid property requirements, feature stability, and resolution. *Annu. Rev. Mater. Res.* **2010**, *40*, 395−414.

(13) Josserand, C.; Thoroddsen, S. T. Drop impact on a solid surface. *Annu. Rev. Fluid. Mech.* **2016**, *48*, 365−391.

(14) Xu, L.; Zhang, W. W.; Nagel, S. R. Drop splashing on a dry smooth surface. *Phys. Rev. Lett.* **2005**, *94*, 184505.

(15) Yu, F.; Lin, S.; Yang, J.; Fan, Y.; Wang, D.; Chen, L.; Deng, X. Prompting Splash Impact on Superamphiphobic Surfaces by Imposing a Viscous Part. *Adv. Sci.* **2020**, *7*, 1902687.

(16) Riboux, G.; Gordillo, J. M. Experiments of drops impacting a smooth solid surface: a model of the critical impact speed for drop splashing. *Phys. Rev. Lett.* **2014**, *113*, 024507.

(17) Liu, Q.; Lo, J. H. Y.; Li, Y.; Liu, Y.; Zhao, J.; Xu, L. The role of drop shape in impact and splash. *Nat. Commun.* **2021**, *12*, 3068.

(18) Bird, J. C.; Dhiman, R.; Kwon, H.-M.; Varanasi, K. K. Reducing the contact time of a bouncing drop. *Nature* **2013**, *503*, 385−388.

(19) Hao, J.; Lu, J.; Lee, L.; Wu, Z.; Hu, G.; Floryan, J. M. Droplet splashing on an inclined surface. *Phys. Rev. Lett.* **2019**, *122*, 054501.

(20) Howland, C. J.; Antkowiak, A.; Castrejón-Pita, J. R.; Howison, S. D.; Oliver, J. M.; Style, R. W.; Castrejón-Pita, A. A. It's harder to splash on soft solids. *Phys. Rev. Lett.* **2016**, *117*, 184502.

(21) Shome, A.; Das, A.; Borbora, A.; Dhar, M.; Manna, U. Role of chemistry in bio-inspired liquid wettability. *Chem. Soc. Rev.* **2022**, *51*, 5452−5497.

(22) Zhu, Z.; Zheng, S.; Peng, S.; Zhao, Y.; Tian, Y. Superlyophilic interfaces and their applications. *Adv. Mater.* **2017**, *29*, 1703120.

(23) Rioboo, R.; Marengo, M.; Tropea, C. Time evolution of liquid drop impact onto solid, dry surfaces. *Exp. Fluids* **2002**, *33*, 112−124.

(24) Scheller, B. L.; Bousfield, D. W. Newtonian drop impact with a solid surface. *AIChE J.* **1995**, *41*, 1357−1367.

(25) de Gennes, P. G. Wetting: Statics and dynamics. *Rev. Mod. Phys.* **1985**, *57*, 827−863.

(26) Biance, A. L.; Clanet, C.; Quéré, D. First steps in the spreading of a liquid droplet. *Phys. Rev. E* **2004**, *69*, 016301.

(27) Wang, Y.; Di, J. C.; Wang, L.; Li, X.; Wang, N.; Wang, B. X.; Tian, Y.; Jiang, L.; Yu, J. H. Infused-liquid-switchable porous nanofibrous membranes for multiphase liquid separation. *Nat. Commun.* **2017**, *8*, 575.

(28) Chen, Y.; Zhu, Z.; Jiang, X.; Jiang, L. Construction of Free-Standing MOF Sheets through Electrochemical Printing on Superhydrophobic Substrates. *ACS Mater. Lett.* **2022**, *4*, 609−617.

(29) Tanner, L. The spreading of silicone oil drops on horizontal surfaces. *J. Phys. D: Appl. Phys.* **1979**, *12*, 1473−1484.

(30) Heslot, F.; Fraysse, N.; Cazabat, A. Molecular layering in the spreading of wetting liquid drops. *Nature* **1989**, *338*, 640−642.

(31) Overney, R. M.; Meyer, E.; Frommer, J.; Brodbeck, D.; Luthi, R.; Howald, L.; Güntherodt, H. J.; Fujihira, M.; Takano, H.; Gotoh, Y. Friction measurements on phase-separated thin films with a modified atomic force microscope. *Nature* **1992**, *359*, 133−135.

(32) Wilbur, J. L.; Biebuyck, H. A.; MacDonald, J. C.; Whitesides, G. M. Scanning force microscopies can image patterned self-assembled monolayers. *Langmuir* **1995**, *11*, 825−831.

(33) Masteika, V.; Kowal, J.; Braithwaite, N. S. J.; Rogers, T. A review of hydrophilic silicon wafer bonding. *ECS J. Solid State Sci. Technol.* **2014**, *3*, Q42−Q54.

(34) Zhu, Z. P.; Tian, Y.; Chen, Y. P.; Gu, Z.; Wang, S. T.; Jiang, L. Superamphiphilic silicon wafer surfaces and applications for uniform polymer film fabrication. *Angew. Chem., Int. Ed.* **2017**, *56*, 5720−5724.

(35) Xu, H.; Shirvanyants, D.; Beers, K.; Matyjaszewski, K.; Rubinstein, M.; Sheiko, S. S. Molecular motion in a spreading precursor film. *Phys. Rev. Lett.* **2004**, *93*, 206103.

(36) Yuan, Q. Z.; Zhao, Y. P. Precursor film in dynamic wetting, electrowetting, and electro-elasto-capillarity. *Phys. Rev. Lett.* **2010**, *104*, 246101.

(37) Kolinski, J. M.; Rubinstein, S. M.; Mandre, S.; Brenner, M. P.; Weitz, D. A.; Mahadevan, L. Skating on a film of air: drops impacting on a surface. *Phys. Rev. Lett.* **2012**, *108*, 074503.

(38) Ledesma-Aguilar, R.; Nistal, R.; Hernandez-Machado, A.; Pagonabarraga, I. Controlled drop emission by wetting properties in driven liquid filaments. *Nat. Mater.* **2011**, *10*, 367−371.

(39) Wang, L.; Zhao, Y.; Tian, Y.; Jiang, L. A general strategy for the separation of immiscible organic liquids by manipulating the surface tensions of nanofibrous membranes. *Angew. Chem., Int. Ed.* **2015**, *54*, 14732−14737.

Supporting Information

Ultrafast Impact Superspreading on Superamphiphilic Silicon Surfaces for Effective Thermal Management

Zhongpeng Zhu,[1,2] Yupeng Chen,[5] Xianfeng Luo,[3,4] Weining Miao,[3,4] Zhichao Dong,[3,4] Jiajia Zhou,[6] Ye Tian,[*,3,4] Lei Jiang[1,2,3,4]

[1] University of Science and Technology of China, Hefei, 230026, China

[2] Suzhou Institute for Advanced Research, University of Science and Technology of China, Jiangsu, 215123, China

[3] Key Laboratory of Bio-inspired Materials and Interfacial Science, Technical Institute of Physics and Chemistry, Chinese Academy of Sciences, Beijing 100190, China

[4] University of Chinese Academy of Sciences, Beijing 100049, China

[5] CAS Key Laboratory for Biomedical Effects of Nanomaterials and Nanosafety, CAS Center for Excellence in Nanosci-ence, National Center for Nanoscience and Technology, Beijing 100190, China

[6] South China Advanced Institute for Soft Matter Science and Technology, School of Emergent Soft Matter, South China University of Technology, Guangzhou 510640, China

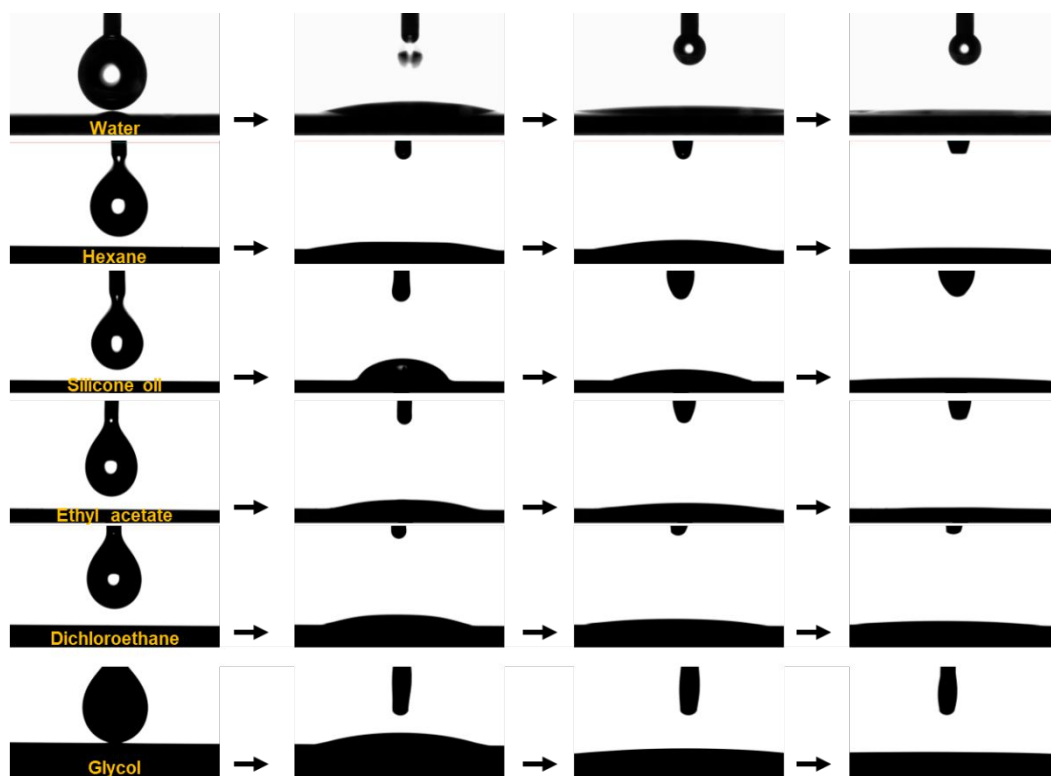* E-mail: tianyely@iccas.ac.cn

Table of Contents

Figure S1 Contact angle measurements of various liquids on superamphiphilic (SAPL) silicon surfaces.
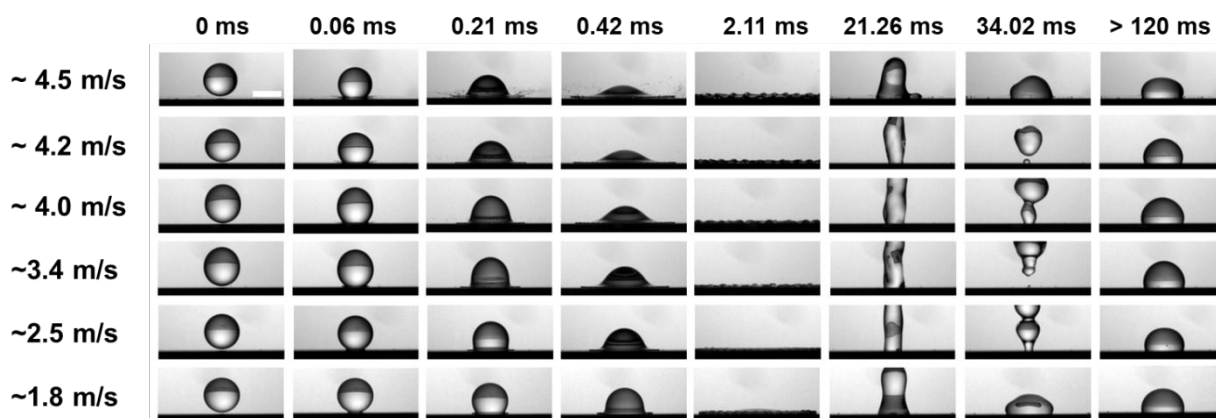
Figure S2 Water droplet impacts on hydrophobic (HPB) surfaces with different impact velocities. Eight typical moments are selected to show the impact rebound behaviors of water droplets at different velocities on HPB silicon surfaces (Scale bar is 2.0 μm).
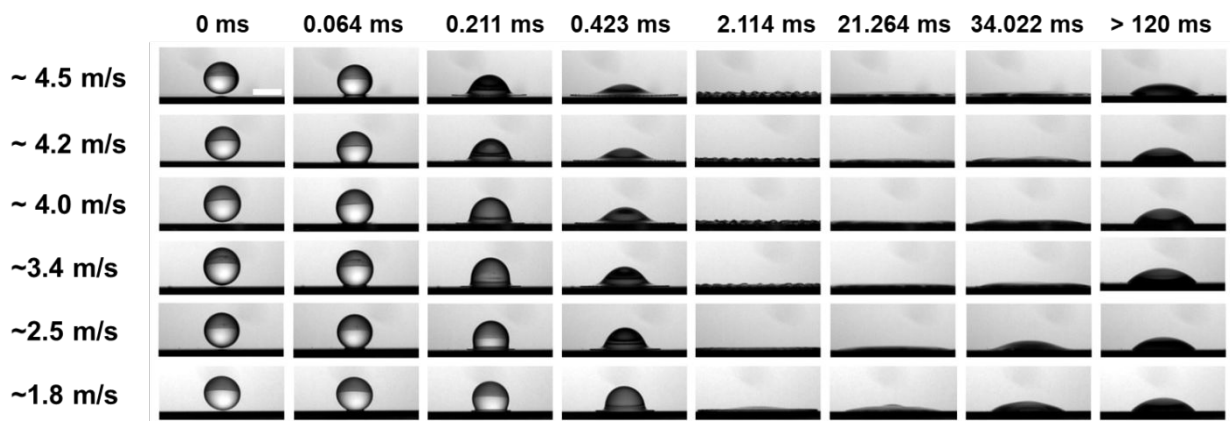
Figure S3 Water droplet impacts on hydrophilic (HPL) surfaces with different impact velocities. Eight typical moments are selected to show the impact with retraction behaviors of water droplets at different velocities on HPL silicon surfaces (Scale bar is 2.0 μm).
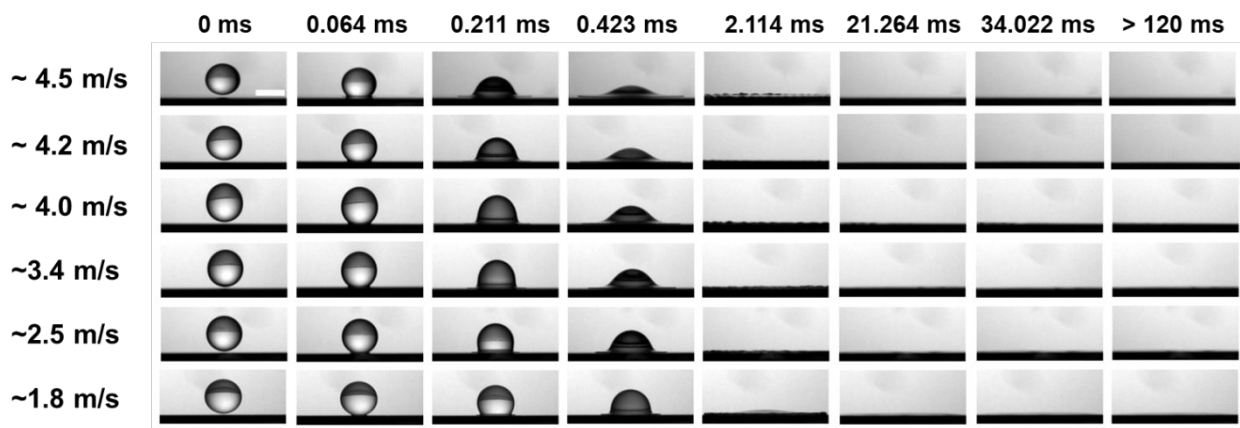
Figure S4 Water droplet impacts on SAPL surfaces with different impact velocities. Eight typical moments are selected to show the impact superspreading behaviors of water droplets at different velocities on SAPL silicon surfaces (Scale bar is 2.0 μm).
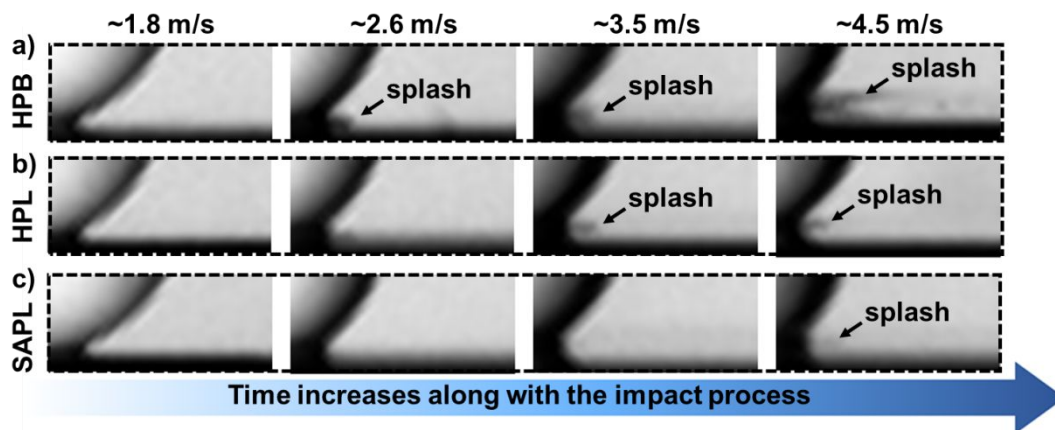
Figure S5 Comparison of the initial splash process at 0.064 ms after water droplets impact on HPB, HPL, and SAPL surfaces with four distinct impact speeds. a) The initial splash occurs at an impact speed of ~2.6 m/s on HPB surfaces. b) The initial splash occurs at an impact speed of ~3.5 m/s on HPL surfaces. c) The initial splash occurs at an impact speed of ~4.5 m/s on SAPL surfaces.
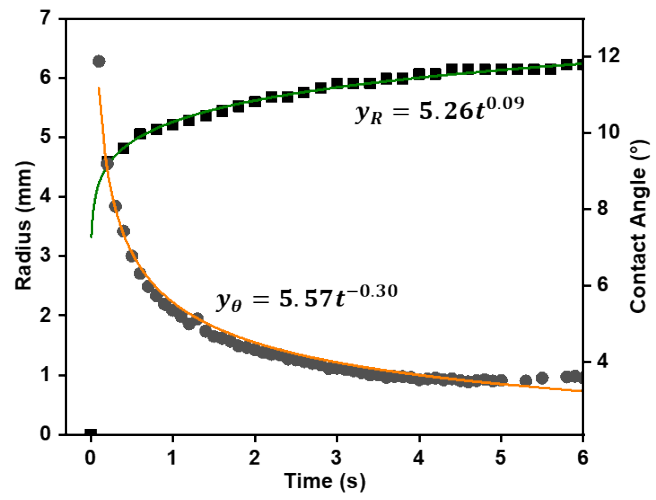
Figure S6 The spreading factors can be calculated based on radius versus time curve or contact angle versus time curve. When the liquid spreading process follows the Tanner's Law, the spreading factor will be around -0.3 (calculated based on contact angle) and 0.1 (calculated based on radius).

The blue circle, gray triangle, and red cross represent non-splash, transition, and splash, respectively. It is intriguing to find that for liquid with relatively high impact speed, the effective suppression can be achieved on HPL and SAPL surfaces (water, dimethyl sulphoxide, hexane). However, when impact speed decreases to 2.0 m/s, the influence of surface wettability is hard to observe (hexadecane and ethanol), and impact speed becomes the dominant factor determining the impact behaviors.

Speed (m/s)	Water 72 mN/m			Dimethyl Sulphoxide 43.6 mN/m			Hexadecane 27.2 mN/m			Ethanol 22.1 mN/m			Hexane 18.4 mN/m		
	HPB	HPL	SAPL	HPB	HPL	SAPL	HPB	HPL	SAPL	HPB	HPL	SAPL	HPB	HPL	SAPL
1.4	O	O	O	O	O	O	O	O	O	O	O	O	O	O	O
1.9	O	O	O	O	O	O	O	O	O	O	O	O	O	O	O
2.0	O	O	O	O	O	O	Δ	Δ	Δ	X	X	X	O	O	O
2.4	O	O	O	X	Δ	O	X	X	X	X	X	X	O	O	O
2.8	O	O	O	X	X	X	X	X	X	X	X	X	O	O	O
3.4	O	O	O	X	X	X	X	X	X	X	X	X	O	O	O
3.7	O	O	O	X	X	X	X	X	X	X	X	X	X	Δ	O
4.0	O	O	O	X	X	X	X	X	X	X	X	X	X	X	X
4.6	X	O	O	X	X	X	X	X	X	X	X	X	X	X	X

X: Splash; Δ: Transition; O: Non-splash;

HPB: Hydrophobic; HPL: Hydrophilic; SAPL: Superamphiphilic.

Figure T1 The impact behavior of various liquids with different surface energy and impact speeds recorded by a high-speed camera on HPB, HPL, and SAPL substrates.